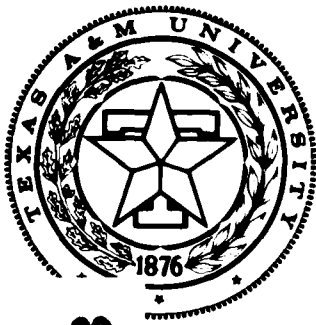


MICROCOPY RESOLUTION TEST CHART
NATIONAL BUREAU OF STANDARDS-1963-A

1

Mechanics and Materials Center
TEXAS A&M UNIVERSITY
College Station, Texas



AD-A165 728

A MICROMECHANICS MODEL FOR NONLINEAR VISCOELASTIC
BEHAVIOR OF PARTICLE-REINFORCED RUBBER WITH
DISTRIBUTED DAMAGE

R. A. SCHAPERY

DTIC
ELECTE
MAR 20 1986
S B D

OFFICE OF NAVAL RESEARCH
DEPARTMENT OF THE NAVY
CONTRACT N00014-83-K-0211
WORK UNIT NR 064-520

MM 4867-86-1

JANUARY 1986

DISTRIBUTION STATEMENT A
Approved for public release
Distribution Unlimited

unclassified

AD-A165728

SECURITY CLASSIFICATION OF THIS PAGE

REPORT DOCUMENTATION PAGE

1a. REPORT SECURITY CLASSIFICATION unclassified		1b. RESTRICTIVE MARKINGS	
2a. SECURITY CLASSIFICATION AUTHORITY		3. DISTRIBUTION/AVAILABILITY STATEMENT DISTRIBUTION STATEMENT A Approved for public release Distribution Unlimited	
2b. DECLASSIFICATION/DOWNGRADING SCHEDULE		unlimited	
4. PERFORMING ORGANIZATION REPORT NUMBER(S) MM-4867-86-1		5. MONITORING ORGANIZATION REPORT NUMBER(S)	
6a. NAME OF PERFORMING ORGANIZATION Mechanics & Materials Ctr. Texas A&M University	6b. OFFICE SYMBOL (if applicable)	7a. NAME OF MONITORING ORGANIZATION ONR	
6c. ADDRESS (City, State and ZIP Code) College Station, Texas 77843		7b. ADDRESS (City, State and ZIP Code)	
8a. NAME OF FUNDING/SPONSORING ORGANIZATION ONR	8b. OFFICE SYMBOL (if applicable)	8. PROCUREMENT INSTRUMENT IDENTIFICATION NUMBER Contract N00014-83-K-0211	
8c. ADDRESS (City, State and ZIP Code) Mechanics Division Office of Naval Research/Code 432 800 N. Quincy Street Arlington, VA 22217		10. SOURCE OF FUNDING NOS.	
11. TITLE (Include Security Classification) Model for Nonlinear Viscoelastic Behavior of Particle-Reinforced Rubber with Distributed		PROGRAM ELEMENT NO.	PROJECT NO.
12. PERSONAL AUTHOR(S) R.A. Schapery		TASK NO.	WORK UNIT NO. 064-520
13a. TYPE OF REPORT Technical	13b. TIME COVERED FROM _____ TO _____	14. DATE OF REPORT (Yr., Mo., Day) January 1986	
15. PAGE COUNT 48			
16. SUPPLEMENTARY NOTATION			
17. COSATI CODES		18. SUBJECT TERMS (Continue on reverse if necessary and identify by block number)	
FIELD	GROUP	Viscoelasticity	
	SUB. GR.	Effective Composite Properties	
		Particulate Composites	
		Solid Propellant	
		Micromechanics	
19. ABSTRACT (Continue on reverse if necessary and identify by block number) A model based on micromechanics for predicting effective viscoelastic stress-strain equations and microcrack growth in particle-reinforced rubber (or other relatively soft viscoelastic matrix) is described. Geometric idealization of the microstructure follows that of the composite spheres assemblage and generalized self-consistent scheme originally used for linear elastic composites without damage. The approach combines a perturbation analysis of the matrix, which becomes more accurate as the particle volume fraction is increased, with the Rayleigh-Ritz energy method for predicting mechanical response of the composite. Results for linear elastic behavior with crack growth are first obtained, and then extensions to linear and nonlinear viscoelastic behavior are discussed. It is shown that the elasticity theory may be easily extended to predict mechanical response of a viscoelastic composite, and that an approximate equation governing microcrack growth is analogous to one for an aging elastic material. Finally, a limited assessment of the theory is made through comparison with some existing effective modulus results and experimental data on a particle-filled rubber.			
20. DISTRIBUTION/AVAILABILITY OF ABSTRACT UNCLASSIFIED/UNLIMITED <input checked="" type="checkbox"/> SAME AS RPT. <input type="checkbox"/> DTIC USERS <input type="checkbox"/>		21. ABSTRACT SECURITY CLASSIFICATION unclassified	
22a. NAME OF RESPONSIBLE INDIVIDUAL Dr. Alan Kushner		22b. TELEPHONE NUMBER (Include Area Code) (202) 696-4305	22c. OFFICE SYMBOL

A MICROMECHANICS MODEL FOR NONLINEAR VISCOELASTIC BEHAVIOR OF
PARTICLE-REINFORCED RUBBER WITH DISTRIBUTED DAMAGE

R. A. Schapery

Texas A&M University

College Station, TX 77843

ABSTRACT

mathematical
A model based on micromechanics for predicting effective viscoelastic stress-strain equations and microcrack growth in particle-reinforced rubber (or other relatively soft viscoelastic matrix) is described. Geometric idealization of the microstructure follows that of the composite spheres assemblage and generalized self-consistent scheme originally used for linear elastic composites without damage. The approach combines a perturbation analysis of the matrix, which becomes more accurate as the particle volume fraction is increased, with the Rayleigh-Ritz energy method for predicting mechanical response of the composite. Results for linear elastic behavior with crack growth are first obtained, and then extensions to linear and nonlinear viscoelastic behavior are discussed. It is shown that the elasticity theory may be easily extended to predict mechanical response of a viscoelastic composite, and that an approximate equation governing microcrack growth is analogous to one for an aging elastic material. Finally, a limited assessment of the theory is made through comparison with some existing effective modulus results and experimental data on a particle-filled rubber.

S DTIC ELECTE **D**
MAR 20 1986
B



✓	
Approved for Release	
Dist	
A-1	

1. Introduction

Rubber which is filled with a large volume fraction of hard particles usually exhibits considerable nonlinearity and strain rate-dependent hysteresis over a wide range of temperatures and rates. In this paper we develop a mathematical model from micromechanical considerations for predicting the growth of microcracks and their effect on the elastic and viscoelastic deformation behavior of such a composite. Motivation for the geometric idealizations and analytical approach comes from studies of the constitutive behavior and microstructure of composite solid propellant. However, it should be clear that at least portions of the theory may apply to many other composites consisting of continuous matrices reinforced with a large volume fraction of much stiffer and stronger particles or fibers; in the latter case prediction of response characteristics for loading transverse to the fibers would be analogous to that done here.

Figure 1 shows the microstructure of a typical composite solid propellant [1]. In this case there is 76 volume percent filler consisting primarily of ammonium perchlorate particles with some aluminum powder (both of comparable stiffness) in a lightly crosslinked rubber. The applied strain is approximately 30 percent, and is close to that producing specimen failure. Only the largest particles may be easily seen as there is a broad distribution of sizes, primarily in the 10 to 100 micron range. Each particle is surrounded by a strongly attached rubber layer. Typically, beginning at strains that are less than 10 percent of the ultimate value, crack-like voids start to appear near the largest particles and grow steadily and separately from one another; a crack that grows around one large particle does not usually join with other cracks (until the ultimate strain is approached) because of the shielding effect of adjacent particles.

Uniaxial stress-strain behavior of a similar propellant (with 78 volume

percent particles) is shown in Fig. 2 over a two minute test period. The points are experimental values and the continuous line is from the equation developed in [2]. One specimen grip was allowed to slip in compression (with respect to the machine crosshead) to avoid buckling of the long bar-shaped specimen; the data points reflect this low compressive resistance. On the basis of the earlier study [2], data on dilatation of propellant [3], and the characteristic behavior of stronger rubber with and without particles [4], it is believed the stress-strain behavior in Fig. 2 reflects hysteresis due to viscoelasticity (the difference between curves 2 and 3), stiffening due to high axial straining of at least a fraction of the polymer network chains (the upper end of curve 3), softening due to microcracks, and the type of softening usually called the Mullins' Effect. This latter phenomenon, which is very significant in carbon black-filled rubber without apparent microcracking, is believed to be primarily due to non-affine displacement of network junctions and entanglements during loading, followed by partial or delayed recovery of these points at reduced strains; with weak crosslinks, more or less permanent breakdown of network junctions may also occur [4]. Figure 3 illustrates the Mullins' Effect without viscoelastic hysteresis.

In view of these several apparently important mechanisms of inelastic behavior which influence mechanical response of the composite, it is believed essential to begin our study with a highly simplified microstructural geometry. When the effects of the different mechanisms are understood, less idealized geometry may be introduced as necessary. Accordingly, as a starting point, we shall use a geometry originally proposed by Kerner [5] for isotropic, linear elastic media without cracks, which is illustrated in Fig. 4. A two-phase composite sphere, consisting of a spherical particle and matrix shell, is embedded in an effective (homogeneous) medium in Kerner's

model. The bulk and shear moduli of the effective medium are initially unknown; but they are found from the condition that the total composite body in Fig. 4, consisting of the two-phase sphere in the much larger effective medium, is to have the same moduli as the effective medium. Hashin [6] calls this model the "generalized self-consistent scheme". Corrections and improvements to this linear model have been made by Smith [7] and Christensen and Lo [8]; additional discussion and comparison with experimental data may be found in [9]. If the displacements specified on the outer boundary of the effective continuum are those for a uniformly strained homogeneous body in simple shear, for example, then the effective shear modulus may be found. Instead, if displacements for simple shear are applied directly to the outer surface of the matrix shell, then one obtains the upper bound to the shear modulus for Hashin's composite spheres assemblage [10]. Both locations for the boundary conditions are considered in this paper, although expressed in terms of applied displacements which produce axisymmetric deformation in order to simplify the analysis when cracks exist.

In Section 2 we propose a modification of the geometry in Fig. 4 to allow for cracks and then outline the method of analysis. Sections 3-5 give details of the approach, which consists of a combination of perturbation analysis, Rayleigh-Ritz approximate energy method, and fracture mechanics. Rigid particles and linear elastic, incompressible behavior of the matrix are assumed for most of the work in this paper in order to develop, with a minimum of complexity, a mathematical model that has some of the important features of the actual composite and to gain insight for generalizing the analysis. Nonlinear and viscoelastic effects in the matrix are discussed briefly in Sections 6-8. Finally, some numerical results and comparisons are given in Section 9.

2. Description of the Model

The complex geometry of an actual particulate composite, such as that in Fig. 1, is idealized using the geometry in Fig. 5. A representative particle is assumed to be spherical. It is contained in a concentric shell of matrix material, $a < r < b$, which may have one or more cracks. This composite spherical particle is embedded in an uncracked shell of an effectively homogeneous isotropic material, $b < r < c$, having effective properties of the particulate composite without cracks. Finally, the outer region, $r > c$, is assumed to be large enough to permit treatment as being infinite in extent; it is considered to be effectively homogeneous with the effective anisotropic properties of the composite with particles and cracks, but this paper does not explicitly account for the outer region. The thickness of the shell without cracks, $b < r < c$, depends on the microcrack density in the total composite, which is related to the size distribution of particles. Namely, cracks tend to form and grow around the largest particles. In the real composite each large particle with at least one adjacent matrix crack is surrounded locally by composite material consisting of smaller particles in apparently uncracked matrix material; it is this latter material that is represented by the shell $b < r < c$. The total composite could be thought of as an assemblage of composite regions, $r < c$, each of which contains one large particle with one or more adjacent cracks; if necessary, one could allow for a distribution of sizes, considering variations in a, b , and c .

As in other types of self-consistent models, the composite model in Fig. 5 is subjected to outer boundary displacements at $r \gg c$ which correspond to those for a uniform strain field. The displacement components u_i ($i=1,2,3$) referred to an orthogonal set of Cartesian

coordinates x_i are, for the far-field,

$$u_i = \epsilon_{ij} x_j \quad (1)$$

where $\epsilon_{ij} = \epsilon_{ji}$ are the components of a spacewise constant strain tensor. (The summation convention is employed in which summation over the range of a repeated index is implied.) This displacement representation is completely general for small or large strains, apart from rigid body translation and rotation. The latter motion may be included by adding constants and using nonsymmetric coefficients ϵ_{ij} in Eq. (1) [11]. In developing stress-strain equations it is of course not necessary to include the rigid body motion.

For simplicity we shall consider here only small strain theory and displacements which are symmetrical with respect to the x_3 axis in Fig. 6. There may be one or two axisymmetrical cracks, each centered at one of the poles, as in Fig. 5. For this axisymmetrical deformation case, $\epsilon_{22} = \epsilon_{11}$ and $\epsilon_{12} = \epsilon_{13} = \epsilon_{23} = 0$, so that Eq. (1) in terms of the spherical coordinates becomes

$$u_1 = r \epsilon_{11} \sin \theta \cos \phi, \quad u_2 = r \epsilon_{11} \sin \theta \sin \phi, \quad u_3 = r \epsilon_{33} \cos \theta \quad (2)$$

The displacements in the radial and latitudinal directions, respectively, are found to be

$$u_r = r[e_v/3 + e_d(2 \cos^2 \theta - \sin^2 \theta)/2] \quad (3a)$$

$$u_\theta = -3re_d(\cos \theta \sin \theta)/2 \quad (3b)$$

where e_v and e_d are the dilatation and deviatoric strain, respectively,

$$e_v \equiv 2\epsilon_{11} + \epsilon_{33}, \quad e_d \equiv 2(\epsilon_{33} - \epsilon_{11})/3 \quad (4)$$

Use of the measures of strain defined in Eq. (4), rather than ϵ_{11} and ϵ_{33} , is helpful in the subsequent analysis.

In order to solve the problem of Fig. 5, one makes the displacements in the outer region equal those in Eq. (3) at $r \gg c$, as is done for the problem in Fig. 4. Without cracks, the problems in Figs. 4 and 5 obviously are the same. In this case, the exact linear elastic solution for the mechanical state and the effective Young's modulus may be obtained just as for simple shear [9] by a separation of variables method in which the particle and each shell have the same form of solution. In fact, one finds that the dependence of the displacements on θ is that in Eq. (3) (which is from the uniform strain field) but functions of r appear in place of e_v and e_d ; the function of r which replaces e_d in Eq. (3a) is in general different from that replacing e_d in Eq. (3b). Each shell and the particle has this form of displacement. An analogous situation exists for the stresses.

With cracks this simplicity certainly does not exist for exact solutions. However, we shall use it for developing approximate solutions based on the minimum potential energy principle. For example, with reference to the inner shell with cracks, $a < r < b$, the interface displacements at $r=b$ are taken as

$$u_r = b[q_1/3 + q_2(2 \cos^2 \theta - \sin^2 \theta)/2] \quad (5a)$$

$$u_\theta = -3b q_3(\cos \theta \sin \theta)/2 \quad (5b)$$

where q_1 , q_2 , q_3 are free parameters which are found by minimizing the strain energy for a given crack geometry. The outer material, $r > b$, then deforms as if there were an uncracked inner shell with altered properties. In practice, for the type of highly-filled, rigid particle system in Fig. 1, the constraining effect of small, closely spaced particles just outside of the soft matrix shell around each large particle tends to preclude high crack-induced displacement gradients for $r > b$. Thus, Eq. (5) may actually

be a more realistic representation than would be the case if the material for $r > b$ were truly homogeneous.

The same form of displacement variation may be used at the interface $r=c$, but with three additional free parameters, also to be found by minimizing the strain energy. However, analysis of the entire composite in Fig. 5 has not yet been completed. Rather, a more limited set of results has been obtained in which displacements in Eq. (3) are applied directly at $r=b$ for one case, and at $r=c$ for another case. With these results, we may determine if the essential characteristics of the model with crack growth agree with experimental data.

Consistent with the limited goal of studying the essential behavior of the model, especially that due to the cracked shell, $a < r < b$, we assume the particles are rigid and the matrix is incompressible. We have done some work, as yet unpublished, allowing for realistic values of rubber compressibility and particle moduli. It was found that only the effects of rubber compressibility on the composite properties were not negligible for the type of composite in Fig. 1; but they were small enough to be neglected in a study of primary model characteristics.

The effective stress-strain equations of the composite will be obtained by evaluating the total strain energy for a unit volume of the composite and then using virtual work to define the stresses,

$$\delta W = \sigma_{ij} \delta \epsilon_{ij} \quad (6)$$

where W is the strain energy per unit volume; W depends on the microcracks, but they are considered to be of fixed length in the virtual deformation process. For axisymmetric deformation and using e_v and e_d in Eq. (4) as the measures of strain, Eq. (6) becomes

$$\delta W = (\sigma_{33} - \sigma_{11}) \delta e_d + (2\sigma_{11} + \sigma_{33}) \delta e_v / 3 \quad (7)$$

which yields the following deviatoric and dilatational equations

$$\sigma_d \equiv \sigma_{33} - \sigma_{11} = \partial W / \partial e_d, \quad \sigma_v \equiv (2\sigma_{11} + \sigma_{33})/3 = \partial W / \partial e_v \quad (8)$$

These results allow for material nonlinearity. For an incompressible composite $e_v = 0$ and only the first relation in Eq. (8) applies; in this case Eq. (4) yields

$$\epsilon_{11} = -\epsilon_{33}/2, \quad e_d = \epsilon_{33} \quad (9)$$

3. Field Equations and Boundary Conditions for the Matrix Shell

Displacement and strain distributions in the matrix shell or layer, $a < r < b$, in Fig. 5 will be constructed for incompressible behavior by deriving the displacements u_r and u_θ from the curl of a vector potential [11]. For symmetry about the x_3 axis, Fig. 6, they become

$$u_r = (r \sin \theta)^{-1} \partial(\psi \sin \theta) / \partial \theta \quad (10)$$

$$u_\theta = -(r \sin \theta)^{-1} \partial(r \psi \sin \theta) / \partial r \quad (11)$$

It is helpful to replace the potential ψ by a dimensionless displacement function,

$$F \equiv r \psi \sin \theta / R^3 \quad (12)$$

where R is the mean radius of the matrix shell, Fig. 7. In addition, for development of a perturbation solution we replace r in favor of the dimensionless radial coordinate x , which is defined by

$$r = (1 + hx)R \quad (13)$$

The dimensionless thickness,

$$h \equiv H/R \quad (14)$$

is assumed to be small enough to use it as a perturbation parameter. Observe that inner and outer radii of the matrix shell are given by $x = -1$ and $x = 1$, respectively. In view of Eq. (13),

$$\partial/\partial r = (Rh)^{-1} \partial/\partial x \quad (15)$$

With a change of variables to F and x , as well as the use of the dimensionless radius,

$$\hat{r} \equiv r/R = 1 + hx \quad (16)$$

Eqs. (10) and (11) become

$$u_r = R \hat{r}^{-2} (\sin \theta)^{-1} \partial F/\partial \theta \quad (17)$$

$$u_\theta = -R(h \hat{r})^{-1} (\sin \theta)^{-1} \partial F/\partial x \quad (18)$$

The strain-displacement equations [11] in terms of the dimensionless variables x and \hat{r} are

$$\epsilon_r = (Rh)^{-1} \partial u_r/\partial x \quad (19a)$$

$$\epsilon_\theta = (R\hat{r})^{-1} (\partial u_\theta/\partial \theta + u_r) \quad (19b)$$

$$\epsilon_\phi = (R\hat{r})^{-1} (u_r + \cot \theta u_\theta) \quad (19c)$$

$$\gamma_{r\theta} = (R\hat{r})^{-1} (\partial u_r/\partial \theta - u_\theta) + (Rh)^{-1} \partial u_\theta/\partial x \quad (19d)$$

Now rewrite the strains using the displacements in Eqs. (17) and (18),

$$\epsilon_r = (h \sin \theta)^{-1} \hat{r}^{-2} [\partial^2 F/\partial \theta \partial x - 2h \hat{r}^{-1} \partial F/\partial \theta] \quad (20a)$$

$$\epsilon_\theta = (h \sin \theta)^{-1} \hat{r}^{-2} [-\partial^2 F/\partial \theta \partial x + \cot \theta \partial F/\partial x + h \hat{r}^{-1} \partial F/\partial \theta] \quad (20b)$$

$$\epsilon_\phi = (h \sin \theta)^{-1} \hat{r}^{-2} [h \hat{r}^{-1} \partial F/\partial \theta - \cot \theta \partial F/\partial x] \quad (20c)$$

$$\gamma_{r\theta} = (h \hat{r})^{-2} (\sin \theta)^{-1} [2h \partial F/\partial x - \hat{r} \partial^2 F/\partial x^2 + h^2 \hat{r}^{-1} (\partial^2 F/\partial \theta^2 - \cot \theta \partial F/\partial \theta)] \quad (20d)$$

The equilibrium equations [11] for the radial and latitudinal directions using the dimensionless variables are, respectively,

$$\hat{r}^{-2} h^{-1} \partial(\hat{r}^3 \sigma_r)/\partial x + (\sin \theta)^{-1} \partial(\sin \theta \sigma_\theta)/\partial \theta - 3\sigma = 0 \quad (21a)$$

$$\hat{r}^{-2} h^{-1} \partial(\hat{r}^3 \sigma_\theta)/\partial x + (\sin \theta)^{-1} \partial(\sin \theta \sigma_\phi)/\partial \theta - \cot \theta \sigma_\phi = 0 \quad (21b)$$

where σ is the mean normal stress,

$$\sigma \equiv (\sigma_r + \sigma_\theta + \sigma_\phi)/3 \quad (22)$$

For a linear, elastic, isotropic matrix, the stress strain equations are

$$\begin{aligned} \sigma_r &= \sigma + 2G\epsilon_r, & \sigma_\theta &= \sigma + 2G\epsilon_\theta \\ \sigma_\phi &= \sigma + 2G\epsilon_\phi, & \tau_{r\theta} &= G\gamma_{r\theta} \end{aligned} \quad (23)$$

where G is the shear modulus. The mean stress σ is not determined by the strains in view of the incompressibility assumption. When the strains, Eq. (20), are substituted into the stresses, Eq. (23), and then the stresses put into Eq. (21), we obtain two differential equations for the mean stress σ and displacement function F .

For a nonlinear elastic material in which the strain energy density depends on the shear strain invariant given in Eq. (61), the stress-strain equations are the same as those in Eq. (23) except G is a function of this strain invariant.

Using Eq. (5), the boundary conditions on the displacements are specified at $x = 1$ as

$$u_r = R(1+h) [q_1/3 + q_2(2 \cos^2 \theta - \sin^2 \theta)/2] \quad (24a)$$

$$u_\theta = -3R(1+h)q_3(\cos \theta \sin \theta)/2 \quad (24b)$$

Allowing for rigid-body vertical translation of the particle, q_4 , the conditions at $x = -1$ are

$$u_r = q_4 \cos \theta \quad (25a)$$

$$u_\theta = -q_4 \sin \theta \quad (25b)$$

4. Perturbation Analysis for a Linear Elastic Matrix Shell

Using a standard method [12], we expand F and other solution functions in a power series in the (assumed) small parameter h ,

$$F = F_0 + h F_1 + h^2 F_2 + \dots \quad (26)$$

The relevant functions are then substituted into the field equations and boundary conditions, and the equations arising from each set of terms of the same order in h are solved sequentially, starting with the lowest order. In using this approach, it is helpful to select the relevant dependent variables in such a way that the lowest order approximations are independent of h . We find from an initial trial of the technique that F_0 is indeed independent of h and that the corresponding normal stresses are $O(h^{-3})$. (Standard notation is used here in that a quantity of n^{th} order in h is denoted by $O(h^n)$ and, by definition, $O(h^n)/h^n$ is bounded as $h \rightarrow 0$) Thus, we introduce the new variables,

$$s \equiv h^3 \sigma, \quad s_r \equiv h^3 \sigma_r, \quad s_\theta \equiv h^3 \sigma_\theta, \quad s_\phi \equiv h^3 \sigma_\phi \quad (27)$$

The modified mean stress s is expanded like F in Eq. (26),

$$s = s_0 + h s_1 + h^2 s_2 + \dots \quad (28)$$

Next, in terms of the series for s and F express the equations of equilibrium, Eq. (21), using Eqs. (20), (23), and (26)-(28), and then combine the terms into groups, each of which is multiplied by a common power in h . Considering those with the h^0 coefficient, the radial and latitudinal equations yield, respectively,

$$\partial s_\theta / \partial x = 0 \quad (29)$$

$$\partial s_\theta / \partial \theta - G(\sin \theta)^{-1} \partial^3 F_\theta / \partial x^3 = 0 \quad (30)$$

Surprisingly, the equations coming from the factor h^1 are the same as Eqs. (29) and (30) except s_1 and F_1 replace s_0 and F_0 , respectively.

The equations arising from h^2 are much more involved, and therefore we shall limit our analysis to the zeroth and first order terms. It is also found that by neglecting terms $O(h^2)$,

$$s_r = s_\theta = s_\phi = s \quad (31)$$

Inasmuch as the zeroth and first order equations of equilibrium have the same form, it is helpful to work instead with the single equation,

$$ds/d\theta - G(\sin \theta)^{-1} \partial^3 F / \partial x^3 = 0 \quad (32)$$

after noting that s is independent of the dimensionless radial coordinate x (cf. Eq. (29)). This equation is readily integrated with respect to x to obtain F ,

$$F = \frac{\sin \theta}{G} \frac{ds}{d\theta} \frac{x^3}{6} + f_2 \frac{x^2}{2} + f_1 x + f_0 \quad (33)$$

The four functions of θ , i.e. $ds/d\theta$, f_0 , f_1 , and f_2 , will be obtained from the four boundary conditions on displacement, Eqs. (24) and (25). To accomplish this, it is helpful to first express the conditions on u_r in terms of F . Thus, by substituting Eq. (24a) into Eq. (17) and integrating with respect to θ we find for $x=1$,

$$F = (1+h)^3 [-q_1(\cos \theta)/3 + q_2(\sin^2 \theta \cos \theta)/2] + k_1 \quad (34)$$

where k_1 is a constant. For $x = -1$,

$$F = \frac{(1-h)^2}{R} \frac{\sin^2 \theta}{2} q_4 + k_2 \quad (35)$$

and k_2 is another constant. From Eqs. (18) and (24b) for $x=1$,

$$\partial F / \partial x = 3 q_3 h(1+h)^2 (\sin^2 \theta \cos \theta) / 2 \quad (36)$$

and from Eqs. (18) and (25b) for $x=-1$,

$$\partial F/\partial x = h(1-h) (\sin^2 \theta) q_4/R \quad (37)$$

Note that these conditions on the latitudinal displacement are $O(h)$; this implies $u_\theta = 0$ at $x = \pm 1$ for the zeroth order solution. Substitution of F , Eq. (33), into the four conditions, Eqs. (34)-(37), gives equations for obtaining the four functions of θ in Eq. (33). Because the u_θ conditions, Eqs. (36) and (37), are $O(h)$ we may replace $(1+h)^2$ and $(1-h)$ by unity since Eq. (33) is only valid up to the first order; consistent with this approximation, in Eqs. (34) and (35) we may use the approximations

$$(1+h)^3 \approx 1+3h, \quad (1-h)^2 \approx 1-2h \quad (38)$$

There results, finally,

$$\frac{ds}{d\theta} = \frac{3G}{2} \left\{ q_1(1+3h) \left(\frac{\cos \theta - c_1}{3 \sin \theta} \right) - \frac{1}{2} [q_2 + 3(q_2 - q_3)h] \sin \theta \cos \theta + \frac{q_4}{2R} \sin \theta \right\} \quad (39)$$

$$f_2 = \frac{3}{4} q_3 h \sin^2 \theta \cos \theta - \frac{q_4 h}{2R} \sin^2 \theta \quad (40)$$

$$f_1 = q_1(1+3h) \left(\frac{c_1 - \cos \theta}{4} \right) + \frac{3}{8} [q_2 + (3q_2 - q_3)h] \sin^2 \theta \cos \theta + \frac{q_4}{2R} \left(h - \frac{3}{4} \right) \sin^2 \theta \quad (41)$$

$$f_0 = -q_1(1+3h) \frac{\cos \theta}{6} + \left[q_2 \left(\frac{1+3h}{4} \right) - \frac{3}{8} q_3 h \right] \sin^2 \theta \cos \theta + \frac{q_4}{4R} (1-h) \sin^2 \theta + c_2 \quad (42)$$

where the unspecified constants of integration k_1 and k_2 have been eliminated in favor of the new constants c_1 and c_2 .

The shear strain, Eq. (20d), is needed for the subsequent energy analysis, and it is found to be

$$\gamma_{r\theta} = (h \hat{r})^{-2} (\sin \theta)^{-1} \left[-\frac{\sin \theta}{G} \frac{ds}{d\theta} x + 2hf_1 - f_2 \right] \quad (43)$$

The latitudinal displacement, Eq. (18), is especially simple if only the zeroth order approximation F_0 is used. For this case we find that it is distributed parabolically in x ,

$$u_\theta \approx \frac{R}{2Gh} \frac{ds}{d\theta} (1-x^2) \quad (44)$$

as illustrated in Fig. 7.

Also, it is to be noted that the mean stress σ is derived by integrating Eq. (39) and then using Eq. (27), $\sigma = sh^{-3}$. The constant c_1 may be found from consideration of the behavior of s ; on the other hand, c_2 has no effect on the mechanical variables and thus may be taken as zero. Observe that there is a singular term $(\sin \theta)^{-1}$ in Eq. (39), which cannot exist in physically meaningful solutions. Removal of this singularity, together with consideration of the mean stress at the ends of the matrix layer (when one or two cracks exist) leads to the solution in terms of q_1 through q_4 .

Without cracks we must set $q_1 = 0$ to remove the singularity and take $q_4 = 0$ to satisfy the obvious symmetry requirement. Use of these conditions in Eq. (39) leads to

$$s = \sigma_0 h^3 - \frac{3G}{8} [q_2 + 3(q_2 - q_3)h] \sin^2 \theta \quad (45)$$

where σ_0 is an arbitrary constant mean stress. With only one crack at the bottom of the particle, cf. Fig. 5, set $c_1 = 1$ to remove the singularity at $\theta = 0$ and obtain

$$s = \sigma_1 h^3 + \frac{3}{2} G \left\{ \frac{q_1}{3} (1+3h) \left[\ln \left(\frac{\sin \theta}{\sin \theta_1} \frac{\tan(\theta_1/2)}{\tan(\theta/2)} \right) \right] \right. \\ \left. - \frac{1}{4} [q_2 + 3(q_2 - q_3)h] (\sin^2 \theta - \sin^2 \theta_1) - \frac{q_4}{2R} (\cos \theta - \cos \theta_1) \right\} \quad (46)$$

where σ_1 is the normal stress applied to the matrix surface at $\theta = \theta_1$; for an internal cavity pressure p_1 , say, $\sigma_1 = -p_1$. Finally, for two cracks of equal size at the top and bottom of the particle, symmetry conditions imply $c_1 = q_4 = 0$, and therefore

$$s = \sigma_1 h^3 + \frac{3}{2} G \left\{ \frac{q_1}{3} (1+3h) \ln \left(\frac{\sin \theta}{\sin \theta_1} \right) \right. \\ \left. - \frac{1}{4} [q_2 + 3(q_2 - q_3)h] (\sin^2 \theta - \sin^2 \theta_1) \right\} \quad (47)$$

If the two cracks are not of equal length or the normal stresses at the ends of a matrix layer with two cracks are not equal, the constant c_1 would be used along with the constant of integration in s to satisfy the normal stress condition at the ends of the matrix layer. Results for this case as well as for additional cracks or voids could be readily obtained, but they will not be given here.

That the perturbation solution permits satisfaction of normal stress boundary conditions at the ends of the matrix layer is very important with incompressible materials. For highly confined material, such as the matrix layer, the error in a normal stress boundary condition does not decay within a few layer thicknesses from the ends; in fact, the value of θ_1 in Eqs. (46) and (47) may have a strong effect on the entire mean stress distribution. In contrast, a shear stress condition cannot be imposed at the ends because there are no remaining free parameters in the perturbation solution for doing this. Unpublished work of the author on problems for which an incompressible material layer is confined between

much stiffer plates shows that the effect of a surface shear stress decays rapidly and is relatively small within a few layer thicknesses from the end. This localized effect would not be expected to significantly effect the overall strain energy and energy release rate predictions made in the next Section.

5. Energy Analysis

The total strain energy for the composite of Fig. 5 may be written in the form

$$W_T = W_1 + W_2 + W_3 \quad (48)$$

The first term $W_1 = W_1(q_i, \theta_0, \theta_1)$, $i = 1$ through 4, is the strain energy of the inner two-phase composite consisting of a particle and a matrix shell, which can be evaluated from the results of the perturbation analysis. The quantity W_2 is the strain energy of the shell $b < r < c$. In the present limited analysis the outer shell $r > c$ is omitted, and the displacements at the surface $r=c$ are specified to be those of a strained continuum using dilatation e_v and deviatoric strain e_d (cf. Eq. (3)). Assuming continuity of displacements Eq. (24) across the interface $r=b$, we may write $W_2 = W_2(e_d, e_v, q_1, q_2, q_3)$. A more involved analysis which includes W_3 would not be needed if $c \gg b$ or if the goal were to obtain an approximate upper bound on effective moduli using the composite spheres assemblage idealization with or without the shell $b < r < c$.

Inasmuch as the matrix and the uncracked outer shell are incompressible, the overall dilatation e_v and volume change of the inner composite, $r < b$, are directly related. The change in volume of the inner composite is

$$\Delta V_1 = 2\pi b^2 \int_0^\pi \sin\theta \, u_r \, d\theta \quad (49)$$

where u_r is given by Eq. (24a). We obtain

$$\Delta V_1 = 4 \pi b^3 q_1 / 3 \quad (50)$$

showing that q_1 is the dilatation of the inner composite, as expected. This volume change is also that of the complete composite sphere $r < c$, so $\Delta V_1 = 4 \pi c^3 e_v / 3$ and

$$q_1 = (c/b)^3 e_v \quad (51)$$

The free parameters q_2 , q_3 and q_4 are selected so as to minimize the total strain energy,

$$\frac{\partial W_T}{\partial q_i} = \frac{\partial W_1}{\partial q_i} + \frac{\partial W_2}{\partial q_i} = 0 \quad \text{for } i = 2, 3, 4 \quad (52)$$

These three conditions and Eq. (51) give, at least implicitly, the relationships

$$q_i = q_i(e_d, e_v, \theta_0, \theta_1) \quad \text{for } i = 1, 2, 3, 4 \quad (53)$$

Energy Release Rate: The crack growth, as defined by a change in θ_0 and θ_1 , will be related to energy release rate, \mathcal{G} . This quantity may be defined basically as the mechanical work per unit of new crack surface area that becomes available at the crack tip during an infinitesimal amount of growth. The area increase used in this definition is the area of new crack surface projected onto the local crack plane, rather than all of the physical surface area that may exist in the damaged material around a crack tip. For an elastic material, the available work is equal to decrease in strain energy for fixed surface displacements (where external loads are applied.) Considering now the bottom crack in Fig. 5 the increase in crack area is $2 \pi R^2 \sin \beta d\beta$. Thus,

$$\begin{aligned} \mathcal{G} &\equiv -\partial W_T / \partial A = -(2\pi R^2 \sin \beta)^{-1} \partial W_T / \partial \beta \\ &= (2\pi R^2 \sin \theta_1)^{-1} \partial W_T / \partial \theta_1 \end{aligned} \quad (54)$$

A similar result is obviously obtained for the top crack. For two cracks which are of equal length ($\theta_0 = \beta$) and which grow simultaneously,

$$\mathcal{G} = -(4\pi R^2 \sin \beta)^{-1} \partial W_T / \partial \beta \quad (55)$$

where $\partial W_T / \partial \beta$ is the derivative for growth of both cracks. From Eqs. (48) (with $W_3 = 0$), (51), and (52), with e_d and e_v fixed,

$$\frac{\partial W_T}{\partial \theta_1} = \sum_{i=2}^4 \left(\frac{\partial W_1}{\partial q_i} + \frac{\partial W_2}{\partial q_i} \right) \frac{\partial q_i}{\partial \theta_1} + \frac{\partial W_1}{\partial \theta_1} = \frac{\partial W_1}{\partial \theta_1} \quad (56)$$

along with a similar result for $\partial W_T / \partial \theta_0$. Thus, to evaluate \mathcal{G} it is sufficient to consider only the change in W_1 for fixed values of the four parameters q_i .

The overall stress-strain equations are those given in Eq. (8), where it should be recalled that the derivatives are taken with the crack sizes fixed and that W is the strain energy per unit volume, W_T/V ; here

$V = 4\pi c^3/3$. Using Eq. (48) without W_3 ,

$$\sigma_d = V^{-1} \left[\sum_{i=2}^4 \left(\frac{\partial W_1}{\partial q_i} + \frac{\partial W_2}{\partial q_i} \right) \frac{\partial q_i}{\partial e_d} + \frac{\partial W_2}{\partial e_d} \right] \quad (57)$$

Introduction of Eq. (52) yields

$$\sigma_d = V^{-1} \partial W_2 / \partial e_d \quad (58)$$

The dilatational equation is derived similarly,

$$\sigma_v = V^{-1} [(c/b)^3 \partial W_1 / \partial q_1 + \partial W_2 / \partial e_v] \quad (59)$$

In differentiating W_2 it is supposed that Eq. (51) has been introduced first so that W_2 does not depend on q_1 .

Use of the Perturbation Solution: The strain energy W_1 is only for the matrix because the particle is assumed rigid. For an incompressible material, the strain energy density of the matrix may be written in the form,

$$w_1 = \frac{1}{2} G \gamma^2 \quad (60)$$

where γ is the "equivalent shear strain"; it is a positive quantity that is proportional to the square root of the second invariant of the strain tensor. For the axisymmetric problem under consideration,

$$\gamma = 2[(\epsilon_r - \epsilon_\theta)^2/6 + (\epsilon_r - \epsilon_\phi)^2/6 + (\epsilon_\theta - \epsilon_\phi)^2/6 + \gamma_{r\theta}^2/4]^{1/2} \quad (61)$$

where the positive square root is to be used. Observe that Eq. (20) implies the normal strain differences squared are $O(h^{-2})$ and $\gamma_{r\theta}^2$ is $O(h^{-4})$. To be consistent with the work in Section 4, we retain only the zeroth and first order terms in h in the quantity $(h^2 \gamma)$, and obtain the very simple result

$$\gamma = |\gamma_{r\theta}| \quad (62)$$

where $|\cdot|$ denotes absolute value, and

$$w_1 = \frac{1}{2} G \gamma_{r\theta}^2 \quad (63)$$

Thus, only the shear strain appreciably affects the strain energy in a thin shell. Now, using Eqs. (13), (16), and (63), as well as the approximation that the strain energy density vanishes in the layer wherever it is cracked (assuming compressive stresses are not acting across the crack surface) yields,

$$\begin{aligned} W_1 &= 2\pi \int_{\theta_0}^{\theta_1} \int_a^b \sin \theta \, r^2 \, w_1 \, dr \, d\theta \\ &= \pi G R^3 h \int_{\theta_0}^{\theta_1} \int_{-1}^1 \sin \theta (1+hx)^2 \gamma_{r\theta}^2 \, dx \, d\theta \end{aligned} \quad (64)$$

Substitute Eq. (43) to find

$$W_1 = \frac{2}{3} \pi G(R/h)^3 \int_{\theta_0}^{\theta_1} \sin \theta (G^{-1} ds/d\theta)^2 d\theta \quad (65)$$

Although $(ds/d\theta)^2$ contains some terms $O(h^2)$ it is algebraically convenient to not explicitly omit them. Using Eq. (39) let us next introduce the quantity $\hat{\gamma}$,

$$\hat{\gamma} \equiv -G^{-1}(ds/d\theta) = \frac{3}{2} \left\{ q_1(1+3h) \left(\frac{c_1 - \cos \theta}{3 \sin \theta} \right) + \frac{1}{2} [q_2 + 3(q_2 - q_3)h] \sin \theta \cos \theta - \frac{q_4}{2R} \sin \theta \right\} \quad (66)$$

Then from Eq. (65),

$$W_1 = \frac{2}{3} \pi G(R/h)^3 \int_{\theta_0}^{\theta_1} \sin \theta \hat{\gamma}^2 d\theta \quad (67)$$

which can be integrated analytically. Also, from Eqs. (54) and (56),

$$\mathcal{G} = G R h^{-3} \hat{\gamma}_1^2 / 3 \quad (68)$$

where $\hat{\gamma}_1 \equiv \hat{\gamma}(\theta_1)$. Recall that $c_1=1$ when $\theta_0 = \alpha$. For two cracks of equal length, $\theta_0 = \beta = \pi - \theta_1$ and $c_1 = q_4 = 0$; we also find from Eqs. (55), (56), and (67) that the energy release rate is again given by Eq. (68).

It is interesting to observe that $\hat{\gamma}_1$ is proportional to the shear strain $\gamma_{r\theta}$, Eq. (43), at the edge of the matrix layer, $\theta = \theta_1$, if the first order term in h , $2hf_1 - f_2$, is neglected. Consequently, with this approximation and Eq. (63), we see that the energy release rate, Eq. (68), is proportional to the strain energy density at $\theta = \theta_1$. This result is analogous to that for strain energy release rate in a long strip between rigid, parallel clamps, in which the strain energy density is that in the uniformly strained portion of the strip [13]. The strain energy available to drive the crack in Fig. 7 is that in the layer just ahead of the tip. Our analysis does not account for details on the scale of h around the

crack tip, and therefore we obtained a result which is like that for the long strip problem. It should be recalled, however, that the simple result in Eq. (68) is valid using both zeroth and first order terms in h , and consequently $\hat{\gamma}_1$ is not limited to proportionality in the local shear strain.

6. Geometric and Material Nonlinearities

The matrix shell analysis made thus far is based on linear theory. Even if global or average strains are not large, the local shear strain is $O(h^{-2})$, Eq. (43), and therefore it may be large in highly-filled composites. However, such behavior does not necessarily invalidate a geometrically linear theory for all but impractically small applied strains. This may be seen by first recognizing that Eqs. (17)-(20) are valid for large deformations if we replace displacements and strains by velocities and strain rates, respectively, and consider r and θ to be Eulerian coordinates and R and H to be instantaneous dimensions. One could then derive displacements by integrating the velocities with respect to time after rewriting the equations in terms of Lagrangian coordinates and the initial geometry. When the displacements are small relative to the respective coordinates, one obtains from this process the same results as now in Eqs. (17), (18), and (20), regardless of the shear strain magnitude. These relative displacements are $O(h^{-1})$ as are the normal strains; but the shear strain is $O(h^{-2})$, thus permitting us to make this distinction between the magnitudes of shear strain and the other measures of deformation.

The shear-strain dominated mode of matrix deformation not only permits the use of the forgoing geometrically linear theory with large shear strains, but, with certain types of material nonlinearity, also leads to mechanical state results which are not much more involved than those for a

fully linear theory. There is not space in this article to cover this topic in detail, and therefore we shall consider it only briefly for a power law nonlinear matrix material characterized by strain energy density

$$w_1 = G_n \gamma^{N+1} / (N+1) \quad (69)$$

where G_n and N are positive constants and γ is the equivalent shear strain, Eq. (61); for $N=1$ Eq. (60) is recovered if we let $G_n = G$. The stress-strain equations arising from Eq. (69) are identical to those in Eq. (23) except G is not constant but instead is given by

$$G = G_n \gamma^{N-1} \quad (70)$$

A perturbation analysis similar to that for the linear case may be employed if modified stresses like those in Eq. (27), but with h^3 replaced by h^{2N+1} , are introduced. Neglecting terms $O(h^2)$ for these modified stresses, the normal stresses are found as before to be equal, Eq. (31), and to be independent of x . Moreover, neglecting terms $O(h)$, the latitudinal equilibrium equation is similar to Eq. (32),

$$ds/d\theta - (\sin \theta)^{-1} \partial(\hat{G} \partial^2 F / \partial x^2) / \partial x = 0 \quad (71)$$

where

$$\hat{G} \equiv G_n (h^2 | \gamma_{r\theta} |)^{N-1} \quad (72)$$

and from Eq. (20d),

$$\hat{G} = G_n [(\sin \theta)^{-1} | \partial^2 F / \partial x^2 |]^{N-1} \quad (73)$$

Equations (71) and (73) lead to results which are analogous to those for the linear case except N appears in the various exponents and coefficients. When terms $O(h)$ are not neglected in the latitudinal equilibrium equation, the results are considerably more involved.

It is of course not necessary to satisfy the equilibrium equations exactly when one uses the minimum strain energy principle to develop approximate solutions. Thus, whether or not terms $O(h)$ are negligible, one could use the zeroth order displacements (i.e., those from Eqs. (71) and (73)) in developing effective stress-strain relations. One could even use the form of the displacement distributions derived from linear theory, but we have found that it is not satisfactory when strong material nonlinearity exists.

7. Viscoelastic Behavior

All of the results obtained so far in this paper may be readily extended to linear and a certain type of nonlinear viscoelastic behavior. The linear viscoelasticity counterpart of the radial stress in Eq. (23), for example, is

$$\sigma_r = \sigma + 2 \int_0^t G(t-t', t) \frac{\partial \epsilon_r}{\partial t'} dt' \quad (74)$$

where $G(t-t', t)$ is the so-called shear relaxation modulus, which imparts hereditary characteristics to the deformation behavior. The second argument in G (i.e. t) allows for aging; this aging may be due to chemical or physical causes, including transient temperature. It is assumed the body is undeformed for $t < 0$, but the lower limit in Eq. (74) and succeeding hereditary integrals should be interpreted as 0^- to allow for the possibility of a discontinuous change in strain or displacement at $t=0$.

Viscoelastic solutions will be derived from elastic solutions through a correspondence principle designated as CP-II in [14]. This principle uses time-dependent solutions rather than Laplace transforms, and is applicable to compressible or incompressible bodies with stationary and growing cracks and with large deformations. With large deformations, the

coordinates r and θ and all dimensions, such as R and h , should be interpreted as quantities which refer to the undeformed geometry. In order to indicate how this correspondence principle would be used here, it is helpful to introduce a so-called pseudo variable,

$$f^R \equiv G_R^{-1} \int_0^t G(t-t', t) \frac{\partial f}{\partial t'} dt' \quad (75)$$

where f represents a displacement-like quantity such as u_r and u_θ , or strain or generalized displacement q_i . With the R superscript, a quantity is called a pseudo displacement or pseudo strain. The coefficient G_R , the "reference modulus", is an arbitrary constant; it is usually selected to have the dimensions of modulus in order for f^R and f to have the same dimensions. The inverse of Eq. (75) is

$$f = G_R \int_0^t J(t-t', t) \frac{\partial f^R}{\partial t'} dt' \quad (76)$$

where J is the shear creep compliance; it is related to G through a hereditary integral [14]. With this notation, Eq. (74) becomes an elastic-like equation,

$$\sigma_r = \sigma + 2G_R \epsilon_r^R \quad (77)$$

A type of nonlinear viscoelastic behavior is characterized through the use of the strain energy density in Eq. (69), but with γ expressed in terms of pseudo strains ϵ_r^R , $\gamma_{r\theta}^R$, etc., instead of the original physical variables. For further discussion of this nonlinear characterization (which includes nonlinear viscous and elastic behavior as special cases) see [14-16].

Let us now explicitly extend the micromechanics analysis to viscoelasticity, beginning with Eq. (1), in which the strains ϵ_{ij} are considered to be specified functions of time. Operate on Eq. (1) with the integral in Eq. (75) to obtain,

$$u_i^R = \varepsilon_{ij}^R x_j \quad (78)$$

According to CP-II, all of the earlier analysis is valid for a viscoelastic material if all displacements and strains are interpreted as pseudo variables; i.e., introduce the superscript R and use G_R for shear modulus (instead of G) as illustrated in Eq. (77). The viscoelastic stresses predicted by this method do not have to be calculated from pseudo stresses; instead, they are simply those in the elastic-like analysis. If boundary tractions instead of the ε_{ij} are specified, then one would solve for ε_{ij}^R from the elastic-like equations in terms of the given tractions, after which the time-dependent strains may be calculated as indicated in Eq. (76).

8. Prediction of Crack Growth

Besides giving a procedure for obtaining viscoelastic solutions from elastic solutions, the theory in [14] provides a method for calculating initiation and continuation of crack growth. We start here with the energy release rate analysis in Section 5; Eq. (68) will be used, in which all displacement-like quantities q_i in $\hat{\gamma}$, Eq. (66), are to be considered as pseudo variables, q_i^R . For simplicity, it is assumed either one crack or two equal-length cracks are in the matrix layer.

It may be helpful to discuss first crack growth in a linear elastic material in which crack growth occurs when a constant "critical" value of energy release rate, \mathcal{G}_c , is reached. The equation for predicting the instantaneous length of one or two equal cracks, as defined by $\beta = \pi - \theta_1$, Fig. 5, follows directly from Eq. (68) after setting $\mathcal{G} = \mathcal{G}_c$,

$$\mathcal{G}_c = G R h^{-3} \hat{\gamma}_1^2 / 3 \quad (79)$$

where, as before, $\hat{\gamma}_1$ is defined by Eq. (66) in which $\theta = \theta_1$. In studies

conducted to date, such as those discussed in Section 9, we have found that the crack growth is stable. That is, as the applied strain is increased (which causes changes in q_i) Eq. (79) yields a unique, increasing crack angle β . This crack growth, in turn, yields decreasing effective shear and bulk moduli, as determined from Eqs. (58) and (59).

The crack growth theory in [14] expresses the growth in terms of a generalized J integral, designated as J_v . For so-called "self-similar" growth [14] (which is concerned with deformation details on the scale of the crack tip) J_v is equal to \mathcal{G} if pseudo-variables, rather than the physical variables, are used. Within the context of the perturbation analysis, the value of \mathcal{G} is not sensitive to the difference between self-similar and more general growth and consequently we shall assume $J_v = \mathcal{G}$. Experience with the type of composite in Fig. 1 indicates that the instantaneous crack speed obeys a power law in \mathcal{G} . For a linear viscoelastic material with a single mode of crack tip deformation, \mathcal{G} is proportional to the square of stress intensity factor; the power law relationship between speed of macrocrack growth and this factor is illustrated in [17] for solid propellant. Thus, it is supposed here that

$$d\beta/dt = (\mathcal{G}/\mathcal{G}_0)^k/t_g \quad (80)$$

where \mathcal{G}_0 is a positive constant with dimensions of energy release rate, and k is a dimensionless, positive constant; the parameter t_g is a positive quantity (with dimension of time) which may vary in time to allow for aging, including transient temperature effects. One may also introduce a crack growth initiation condition, but experience with solid propellant shows that the initiation time is often negligible compared to the total period of crack growth.

As an aid to examining the effect of applied strain history on crack

growth, it is helpful to consider here only those situations for which there is one independently applied strain ϵ , and ϵ and the associated pseudo strain ϵ^R are non-negative. For example, specify a time-dependent axial strain $\epsilon \equiv \epsilon_{33} \geq 0$ and assume the other components, ϵ_{11} and ϵ_{22} , vary proportionally, or are such that a state of average uniaxial tensile stress exists in the x_3 direction. Although other less restrictive cases have been studied, we shall limit our analysis to the aforementioned situations. For each crack length the shear strain parameter $\hat{\gamma}$, Eq. (66), is proportional to ϵ because the problem is linear. Thus, we may write for an elastic material,

$$\hat{\gamma}_1 = \epsilon f(\beta) \quad (81)$$

The function $f = f(\beta)$ is derived by minimizing the strain energy with respect to the free parameters, as discussed in Section 5, and by using the specified transverse straining or loading conditions, such as $\sigma_{11} = \sigma_{22} = 0$. In all cases studied to date we have found that f is a positive, continuous, decreasing function of β . Thus, for each ϵ the elastic energy release rate from Eqs. (68) and (81),

$$\mathcal{G} = G R h^{-3} f^2 \epsilon^{2/3} \quad (82)$$

is a continuous, decreasing function of β . If we assume crack growth occurs when $\mathcal{G} = \mathcal{G}_c$ (assumed constant) and solve Eq. (82) for β as a function of ϵ , we obviously would find that the microcracks grow stably as the applied strain is increased.

For a viscoelastic material, as discussed in Section 7, one replaces G by G_R and ϵ by ϵ^R in Eq. (82), where

$$\epsilon^R \equiv G_R^{-1} \int_0^t G(t-t', t) \frac{d\epsilon}{dt'} dt' \quad (83)$$

Assuming crack growth is defined by Eq. (80),

$$d\beta/dt = (\epsilon^R)^p g/t_g \quad (84)$$

where $p \equiv 2k$ and

$$g = g(\beta) \equiv (G_R R h^{-3} f^2 / 3 \mathcal{G}_0)^k \quad (85)$$

Let us next introduce a "reduced time",

$$\hat{t} = \hat{t}(t) \equiv \int_0^t dt' / t_g(t') \quad (86)$$

Without aging t_g is constant and the reduced time \hat{t} becomes t/t_g .

Integration of Eq. (84) yields

$$\int_{\beta_0}^{\beta} g^{-1} d\beta = S^p \quad (87)$$

where S is the Lebesgue norm of pseudo-strain,

$$S = S(\hat{t}) \equiv \left[\int_0^{\hat{t}} (\epsilon^R)^p d\hat{t}' \right]^{1/p} \quad (88)$$

and β_0 is the initial value of β . Also, $\epsilon^R = \epsilon^R(\hat{t}')$ in Eq. (88), where \hat{t}' is the dummy variable of integration.

Equation (87) may be solved implicitly to obtain the instantaneous crack angle β as a function of the Lebesgue norm S and β_0 . Inasmuch as the value of S determines the amount of crack growth, it will be termed a "damage parameter". Because p is often quite large, it is found that numerical and approximate analytical predictions of β are aided by using the p th root of the integral in Eq. (88) for the damage parameter, rather than S^p as in Eq. (87). It should be noted that when $p \rightarrow \infty$, S becomes the largest value of ϵ^R over all time up to the present [18]. For values $p \geq 4$ and $d\epsilon^R/dt \geq 0$ an excellent approximation is [2],

$$S = \epsilon^R \hat{t}^{1/p} / (p m + 1)^{1/p} \quad (89)$$

where $m \equiv d \log \epsilon^R / d \log \hat{t}$. Similar but somewhat more involved approximations may be constructed for histories ϵ^R which are not monotone increasing in \hat{t} .

In many cases the denominator in Eq. (89) is essentially constant because p is large or m does not vary significantly. If so, the damage parameter depends on only the current value of pseudo strain and time. This behavior enables us to rewrite the basic crack growth equation so that it looks like one for an aging elastic material. Specifically, substitute Eqs. (85) and (89) into Eq. (87), and rewrite it to obtain,

$$\mathcal{G}_{CR} = G_R R h^{-3} (\hat{\gamma}_1^R)^2 / 3 \quad (90)$$

where

$$\hat{\gamma}_1^R \equiv f \epsilon^R \quad (91)$$

$$\mathcal{G}_{CR} \equiv \mathcal{G}_O c^2 f^2 \hat{t}^{-1/k} \left[\int_{\beta_0}^{\beta} f^{-2k} d\beta' \right]^{1/k} \quad (92)$$

and c is the denominator in Eq. (89); recall that $p=2k$. The right side of Eq. (90) has the same form as Eq. (79) for energy release rate in an elastic material. The quantity \mathcal{G}_{CR} thus plays the role of a critical energy release rate; however, instead of being constant, it depends on crack length through β and β_0 and on time. It was observed in Section 7 that the viscoelastic constitutive equations in terms of pseudo strains are analogous to those for an elastic material. Equation (90) shows that this observation extends to crack growth behavior as long as one accounts for crack size and possibly aging in the critical energy release rate.

This elastic-like behavior can be shown to exist when there is more than one independently specified strain or stress. Indeed, using the self-consistent model described in this paper, it leads to the existence of a strain energy-like potential with crack growth. Such behavior is discussed in [19], especially for elastic materials with damage, and an illustration is given using experimental data on solid propellant under confining pressure and axial stretching.

Finally, it should be remarked that there are realistic situations in which the crack growth equation is that in Eq. (80), but the constitutive behavior is that for an elastic material because the shear relaxation modulus is essentially constant. Alternatively, the crack growth equation may be like that for an elastic material, $\mathcal{G} = \text{constant}$, but the relaxation modulus is not constant; this case may be recovered from Eq. (92) by letting $k \rightarrow \infty$.

9. Some Results and Comparisons

Range of Validity of the Perturbation Solution: Without cracks the accuracy of the perturbation analysis in predicting the effective Young's modulus of the composite may be assessed through comparison with certain exact results. We shall consider two cases; for both, it is assumed the particle volume fraction for the composite sphere of radius b in Fig. 4 is the same as that for the total composite. In the first case the displacements in Eq. (3) are applied directly on the surface at $r=b$ in Fig. 4, giving a modulus, denoted by E_b , which may be interpreted as an approximate upper bound to the modulus of Hashin's composite spheres assemblage [10]. The exact expression for this upper bound will be denoted by E_{CS} ; it is three times the shear modulus derived in [10] in view of the incompressibility condition.

To derive E_b we first note that Eq. (24) must be the same as Eq. (3); thus $q_1 = e_v$ and $q_2 = q_3 = e_d$. Moreover, without cracks $e_v = q_4 = 0$, and $e_d = \epsilon_{33}$ from Eq. (9). Equation (66) reduces to

$$\hat{\gamma} = 3 \epsilon_{33} \sin 2\theta / 8 \quad (93)$$

Substitute Eq. (93) into (67), with $\theta_0 = 0$ and $\theta_1 = \pi$, divide the strain energy w_1 by the volume $4\pi b^3/3$, recall that R is the mean radius (cf. Fig. 7), and then use this result for w in the first relation in Eq. (8) with $\sigma_{11} = 0$; there results, finally,

$$\sigma_{33} = E_b \epsilon_{33} \quad (94)$$

where

$$E_b = E/[20n^3(1+3h)] \quad (95)$$

is the composite effective Young's modulus in terms of the matrix Young's modulus, $E=3G$. The third column in Table 1 gives the ratio E_b/E_{CS} for a range of particle volume fractions v_p ; the second column comes from the exact relationship

$$h = (1 - v_p^{1/3})/(1 + v_p^{1/3}) \quad (96)$$

which may be easily derived using the definition for h in Eq. (14). It is encouraging that E_b agrees so well with the exact result E_{CS} for particle volume fractions as low as 0.4.

The second comparison we shall make is for the generalized self-consistent model in Fig. 4, in which boundary displacements in Eq. (3) are applied at a radius $r=c \gg b$. In this case the exact solution for Young's modulus, denoted by E_{SC} , may be obtained from three times the shear modulus in [9, p. 56]. The approximate modulus, say E_C , follows from Eq. (58) with $\sigma_d = \sigma_{33}$, $e_d = \epsilon_{33}$, and $q_4 = e_v = 0$. The strain energy of the effective medium, $r > b$, can be evaluated using exact displacement distributions similar to those in [9]. The process is straightforward and the amount of algebra is considerable. Therefore, only numerical values for the ratio E_C/E_{SC} are given here; they are listed in the fourth column of Table 1. The error in the modulus which uses the perturbation solution is within 13% of the exact solution for $1 - v_p < 0.65$; for the composite in [2] the error is practically zero since $v_p = 0.78$. The last column in Table 1 gives the ratio of exact values, showing that the effective modulus of the generalized self-consistent scheme is considerably smaller than Hashin's upper bound for the v_p range indicated; however, it is found that $E_{SC} > E_{CS}$

as $v_p \rightarrow 0$.

The Perturbation Solution with One Crack: Consider again the case in which the displacements in Eq. (3) are applied on the surface $r=b$, where $\epsilon_{33} > 0$ and $\sigma_{11} = 0$ are the given inputs. We now use both expressions in Eq. (8) to derive σ_{33} and e_v . The strain energy \mathcal{W} is again that in Eq. (67), after dividing by the volume. For $\hat{\gamma}$, Eq. (66), we use $q_1 = e_v$, $q_2 = q_3 = e_d$, $c_1 = 1$, and minimize the strain energy with respect to q_4 to find this particle displacement. The crack angle β is derived from Eq. (79) assuming \mathcal{G}_c is constant.

Figures 8 and 9 show representative distributions of the shear strain measure $\hat{\gamma}$, Eq. (66), and the dimensionless normal stress s/G for three values of the axial strain $\epsilon \equiv \epsilon_{33}$; recall that $s = h^3 \sigma$, Eq. (27), where σ is the normal stress in the matrix. In Fig. 8 the peak values of $\hat{\gamma}$ are the same since \mathcal{G}_c is constant. These plots are for the given values of $\hat{\gamma}_1 = 0.09$ and $v_p = 0.78$ (but the results are not very sensitive to v_p); for the three strains the predicted values of β are approximately 4, 13, and 23 degrees.

Results without a crack are also drawn in Figs. 8 and 9. They are from Eq. (46) (in which $q_1 = q_4 = 0$, $q_2 = q_3 = \epsilon$, and $\theta_1 = \pi$) and from Eq. (93). Without a crack the normal stress at the poles, σ_1 in Eq. (46), is not given by a boundary condition; since the material is incompressible the strains determine the normal stress only to within a constant. This constant may be found by requiring the total radial force/surface area acting on the matrix shell to be the mean applied stress, $\sigma_{33}/3$. With this condition we obtain

$$s/G = [1 + 0.2/(1+3h) - 1.5 \sin^2 \theta] \epsilon / 4 \quad (97)$$

Additional numerical results confirm that the quantity s/G from Eq. (46) for one crack and $\sigma_1=0$ approaches Eq. (97) with decreasing crack length, except near the crack tip. Figures 8 and 9 show that the effect of the crack on $\hat{\gamma}$ and s/G for $\epsilon = 0.05$ is not great except near the tip, and that for all three strains the only qualitative difference in the distributions for no crack, Eqs. (93) and (97), and for one crack is near the crack tip. In additional unpublished studies, the maximum β of 23 degrees in these figures (for $\epsilon = 0.15$) was found to be somewhat larger than needed to achieve agreement with experimental results in [2] on stress-strain behavior; thus, in this case, curves for the largest strain exaggerate the change in the distributions due to crack growth.

Studies with two cracks have been made as well. However, for the same values of G_c and initial crack length as with one crack it is found that a larger value of applied strain is needed to initiate simultaneous propagation. It is thus likely that even if two diametrically opposed cracks were to exist initially, growth of only one would be significant. Comparisons of predicted and measured stress-strain behavior made to-date also support the one-crack model. Predicted stress-strain curves and various comparisons will be published elsewhere.

Effects of Viscoelasticity: Incorporation of viscoelasticity into the model has been discussed in Section 7. Essential aspects of the method for dealing with both crack-tip and global effects are confirmed by the experimental results in [2]. Here we shall discuss only the theoretically derived damage parameter, Eq. (88), and the relationship of this Lebesgue norm to the findings in [2]. Neglecting aging effects, the reduced time \hat{t} , Eq. (86), reduces to $\hat{t} = t/t_g$ in which t_g is a constant. The exponent p is related to the exponent which characterizes time-dependence of the stress

relaxation modulus and to the characteristics of the material in the zone of failing material at a crack tip. For a nonaging material $G(t-t',t)$ reduces to $G(t-t')$, and thus for power law relaxation,

$$G(t) = G_1 t^{-n} \quad (98)$$

where G_1 and n are positive constants. According to the data for rubber in [20:III], the failure zone at the crack tip is elastic-like, which in turn yields [20:II],

$$p = 2(1 + 1/n) \quad (99)$$

This relationship is in agreement with data for macrocrack growth in solid propellant [17]. For the relaxation modulus in [2] $n = 0.366$, and thus $p = 7.46$. From the same study the exponent was found experimentally to be $p = 6.5$. The difference may be in part due to the material nonlinearity; namely, apart from effects of damage, a power law nonlinearity was reported, in which $\sigma_{33} \sim (\epsilon^R)^N$, where $N = 0.85$. In another micromechanics model study it was shown that instead of Eq. (99) one should use $p = (1+N)k$ [16, Eq. (142)]; the quantity k is the same as for a linear viscoelastic material [15], $k = (1+1/n)$. Thus, $p = 6.9$, which is only 6% greater than the experimental value of 6.5.

The experimental data in [2] indicate that two different Lebesgue norms are needed, corresponding to $p = 6.5$ and $p = \infty$, where the latter norm is equal to the largest value of $\epsilon^R(t')$ over all $0 \leq t' \leq t$, where t is the current time [18]. The value $p = \infty$ is what one would predict for an elastic material since $n = 0$. The power law in Eq. (98) with $n = 0.366$ is for a broad, intermediate time range, where in crack growth theory t is one-third the time taken by a crack in growing an amount equal to the length of its crack tip failure zone [20:II]. Thus, considering that there is actually a distribution of particle and microcrack sizes, and associated

microcrack growth rates, the need for $p = \infty$ may arise from the very slow and fast growth rates for which elastic-like behavior would exist. Additionally, molecular scale damage processes related to breakdown of crosslinks and highly entangled long molecular chains (normally associated with the so-called Mullins' effect [4]) may account, at least in part, for the need of the $p = \infty$ value. The value of p may also depend on whether or not the crack tip is in the matrix or at the particle-matrix interface; in this regard it should be noted that the perturbation results are not sensitive to the radial location of the cracks, and thus they apply to both cohesive and adhesive fracture processes. Although it is not yet clear just why $p = \infty$ is needed, it is very encouraging that the two values of $p = 6.5$ and $p = \infty$ bracket the theoretically predicted range of possible exponents using viscoelastic fracture mechanics for the matrix.

With exponents of $p = 6.5$ and larger, corresponding to $k \geq 3.2$, we have found that the value of the effective critical fracture energy, Eq. (92), changes only a small amount with straining except for β very close to its initial value β_0 . Indeed, curves analogous to those in Figs. 8 and 9, but for the viscoelastic material, are practically the same as for elastic behavior. It is also of interest to observe that for $\hat{t} = t/t_g$ and $\epsilon^R = C_1 (t/t_g)^m$, with C_1 and m constant (such as would be obtained for a power law relaxation modulus and a constant strain rate input) we may eliminate \hat{t} from Eq. (92) using

$$\hat{t} = (\epsilon^R/C_1)^{1/m} \quad (100)$$

When this is done the resulting expressions are the same as in Eqs. (90) and (92) except the exponent on $\hat{\gamma}_1^R$ is $2 + 1/mk$, \mathcal{G}_0 is multiplied by $C_1^{1/mk}$, and \mathcal{G}_{CR} no longer depends explicitly on \hat{t} . Namely, the crack growth behavior is predicted to be the same as for a nonlinear power law

elastic material with a strain rate and crack length-dependent fracture energy $\mathcal{G}_{CR} = \mathcal{G}_{CR}(C_1, \beta)$. Also, as a result of the integral in Eq. (92), this energy is initially zero and then initially increases with crack growth.

10. Conclusions

A model has been described for predicting microcrack growth and the overall or effective constitutive equations of a highly-filled particulate composite. Assuming rigid spherical particles and an incompressible matrix, the theory was developed using a combination of perturbation and strain energy methods. Accuracy of the perturbation analysis, which increases with increasing values of particle volume fraction, v_p , was assessed by comparing the effective Young's modulus with existing exact values predicted for the composite spheres assemblage and the generalized self-consistent model. In the latter case the error is less than 13% for $v_p > 0.65$, and in the former case the error is less than 8% for $v_p > 0.40$. Viscoelastic effects were introduced, and a damage parameter that defines the extent of time-dependent microcracking was derived and found to be in good agreement with experimental results on a rubber filled with relatively rigid particles.

This paper described only the basic portion of a much more extensive study underway to predict the mechanical response of linear and nonlinear viscoelastic particulate composites. The geometric idealization of the composite and the method of analysis were selected to be realistic but yet simple enough that it would be feasible to include geometric and material nonlinearities, compressibility of the matrix, and particle deformation under multiaxial loading of the composite. Studies beyond those covered here have been made and will be reported elsewhere.

References

- [1] L.R. Cornwell and R.A. Schapery, SEM study of microcracking in strained solid propellant. Metallography. 8, 445-452 (1975).
- [2] R.A. Schapery, Models for damage growth and fracture in nonlinear viscoelastic particulate composites, Proc. Ninth U.S. National Congress of Applied Mechanics, Book No. H00228, The American Society of Mechanical Engineers, 237-245 (1982).
- [3] R.J. Farris, The influence of vacuole formation on the response and failure of highly filled elastomers. Trans. Soc. Rheol. 12:2, 315-334 (1968).
- [4] L. Mullins, Softening of rubber by deformation. Rubber Chem. Technol. 42, 339-362 (1969).
- [5] E.H. Kerner, The elastic and thermoelastic properties of composite media. Proc. Phys. Soc. B69, 808 (1956).
- [6] Z. Hashin, Analysis of composite materials - a survey. J. Appl. Mech. 50, 481-505 (1983).
- [7] J.C. Smith, Correction and extension of Van der Poel's method for calculating the shear modulus of a particulate composite. J. Res. Nat. Bureau Standards. 78A, 355-362 (1974).
- [8] R.M. Christensen and K.H. Lo, Solutions for effective shear properties in three phase sphere and cylinder models. J. Mech. Phys. Solids. 27, 315-330 (1979).
- [9] R.M. Christensen, Mechanics of Composite Materials. John Wiley and Sons, New York (1979).
- [10] Z. Hashin, The elastic moduli of heterogeneous materials. J. Appl. Mech. 29, 143-150 (1962).

- [11] L.E. Malvern, Introduction to the Mechanics of a Continuous Medium. Prentice-Hall, Inc., Englewood Cliffs, N.J. (1969).
- [12] M.D. Greenberg, Foundations of Applied Mathematics. Prentice-Hall, Inc., Englewood Cliffs, N.J. (1978).
- [13] J.R. Rice, A path independent integral and the approximate analysis of strain concentration by notches and cracks. J. Appl. Mech. 35, 379-386 (1968).
- [14] R.A. Schapery, Correspondence principles and a generalized J integral for large deformation and fracture analysis of viscoelastic media. Int. J. Fracture 25, 195-223 (1984).
- [15] R.A. Schapery, Continuum aspects of crack growth in time-dependent materials. Encyclopedia of Materials Science and Engineering. Pergamon Press LTD, Oxford (1986).
- [16] R.A. Schapery, On viscoelastic deformation and failure behavior of composite materials with distributed flaws. 1981 Advances in Aerospace Structures and Materials - AD-01, S.S. Wang and W.J. Renton, Eds., Am. Soc. Mech. Eng., New York, 5-20 (1981).
- [17] R.A. Schapery, Fracture mechanics of solid propellants. Fracture Mechanics, N. Perrone, H. Liebowitz, D. Mulville, W. Pilkey, Eds. Univ. Press of Virginia, Charlottesville, 387-398, (1973).
- [18] J.N. Reddy and M.L. Rasmussen, Advanced Engineering Analysis. John Wiley & Sons, New York (1982).
- [19] R.A. Schapery, Deformation and fracture characterization of inelastic composite materials using potentials. Texas A&M Univ. Report No. MM-5034-85-22 (1985).
- [20] R.A. Schapery, A theory of crack initiation and growth in viscoelastic media. Int. J. Fracture 11, Part II, 369-388; Part III, 549-562 (1975).

Table 1

Effective Modulus Ratios for Composite Spheres Assemblage (CS)
and Generalized Self-Consistent Scheme (SC).

v_p	h	E_D/E_{CS}	E_C/E_{SC}	E_{SC}/E_{CS}
.999	1.67×10^{-4}	1.00	1.00	.624
.9	.0176	1.00	1.00	.556
.8	.0372	1.00	1.00	.475
.7	.0594	1.00	.94	.390
.65	.0717	.99	.87	.352
.6	.0849	.99	.72	.326
.5	.115	.97	.21	.322
.4	.152	.92	< 0	.379



Figure 1. Microtoned surface of a thin sheet of propellant under uniaxial stress (in the direction of the arrow) just below that causing specimen failure, as observed through a scanning electron microscope (100X). After Cornwell and Schapery [1].

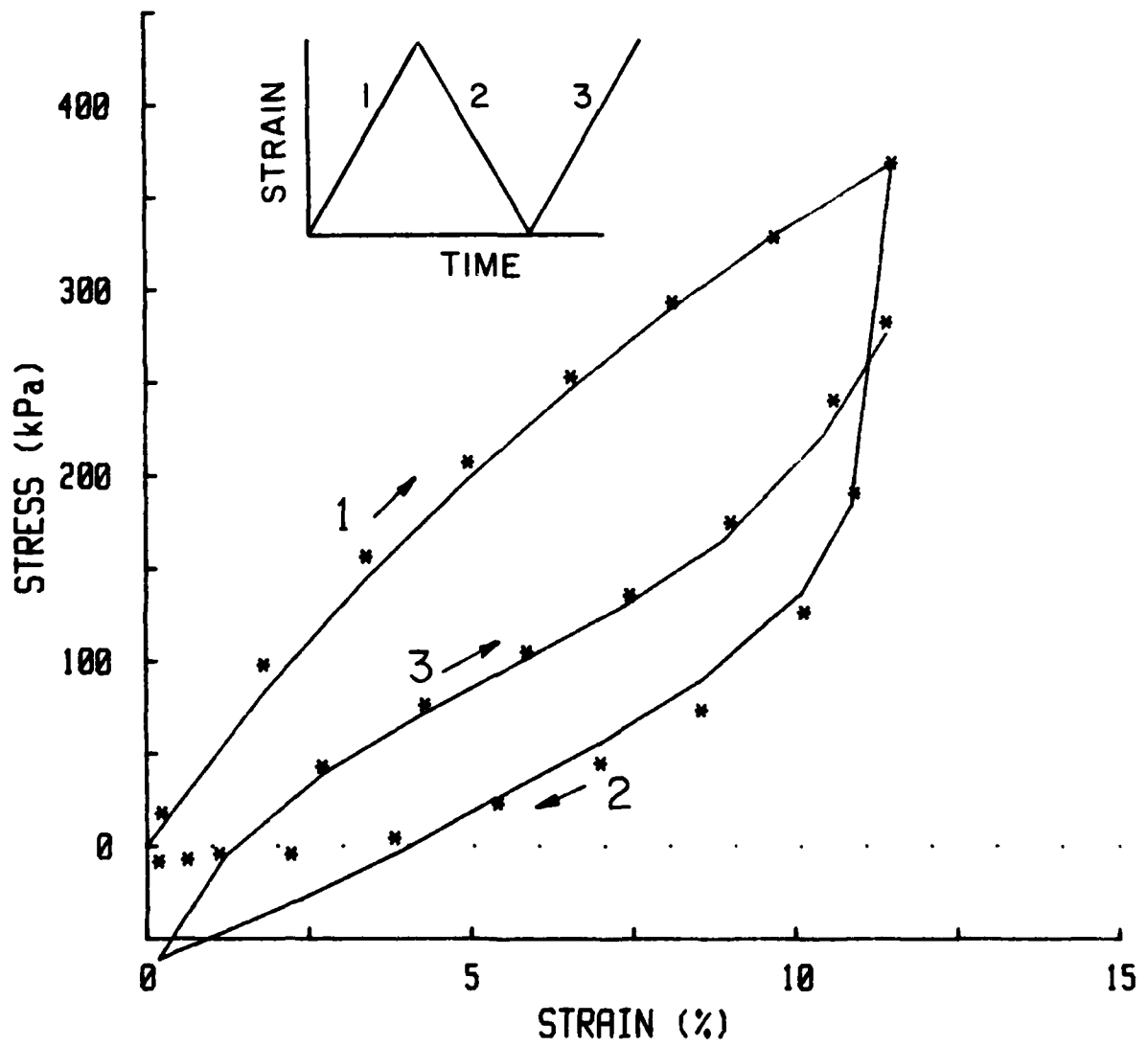


Figure 2. Stress-strain curves for a filled rubber similar to that in Figure 1. After Schapery [2].

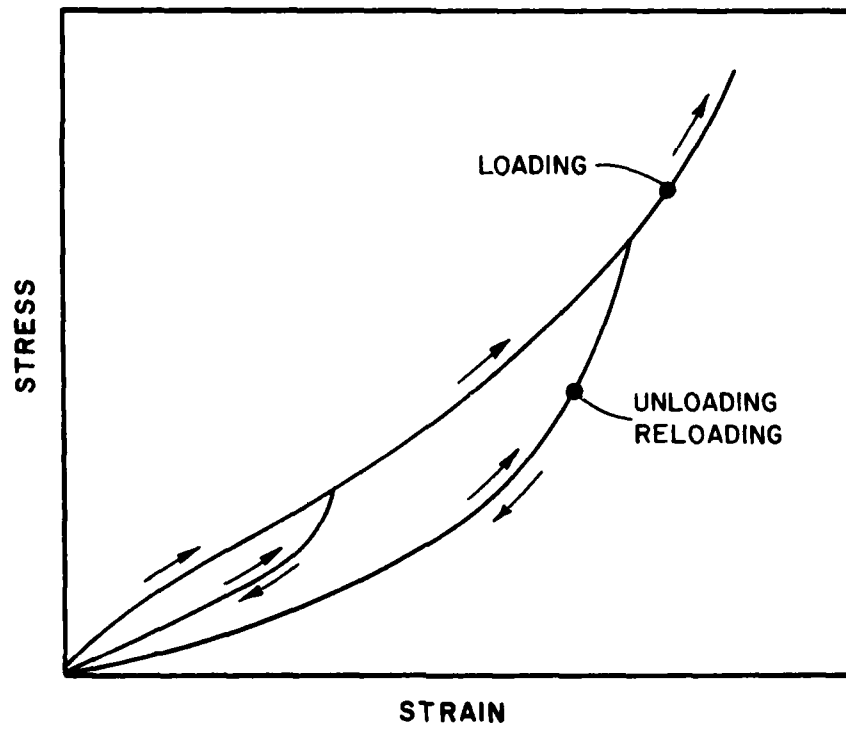


Figure 3. Illustration of the Mullins' Effect in filled rubber without viscoelasticity and microcracking.

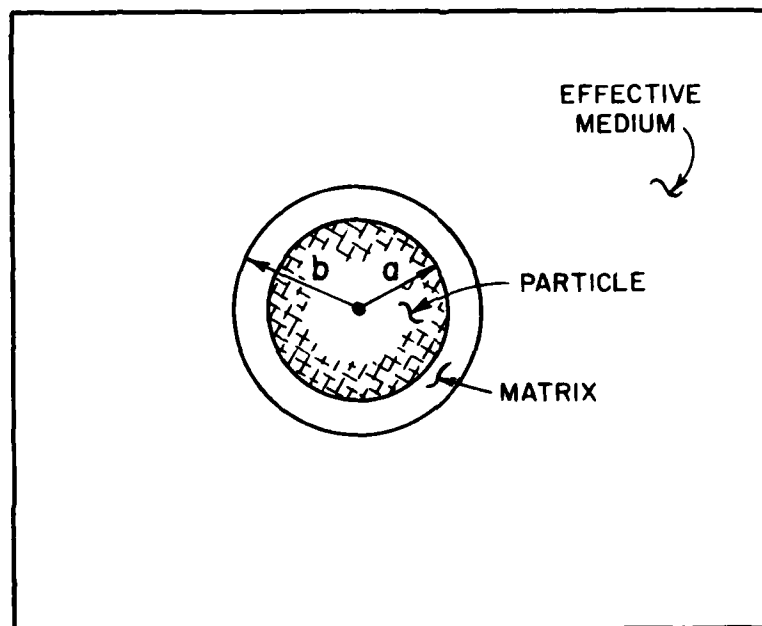


Figure 4. Generalized self-consistent scheme without microcracking.

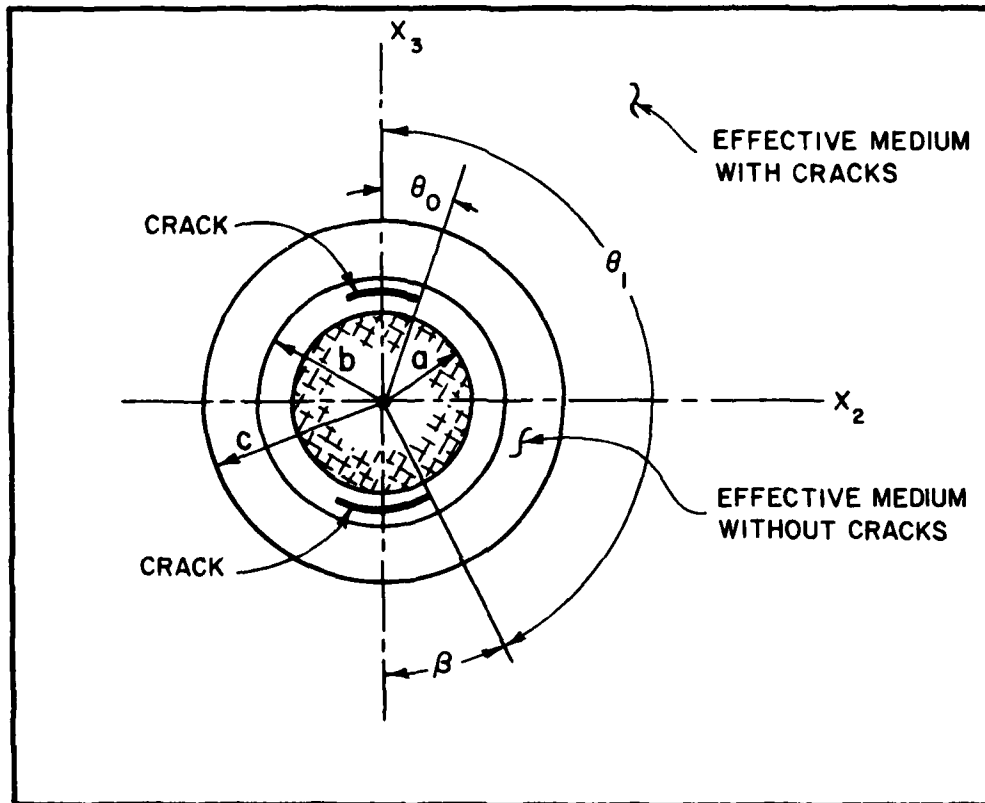


Figure 5. Generalized self-consistent scheme with microcracking.

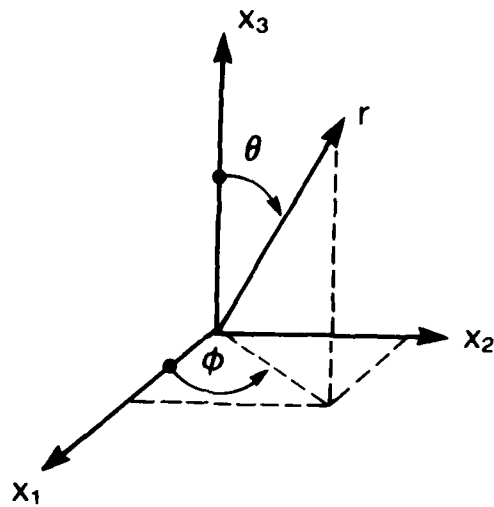


Figure 6. Spherical coordinate system.

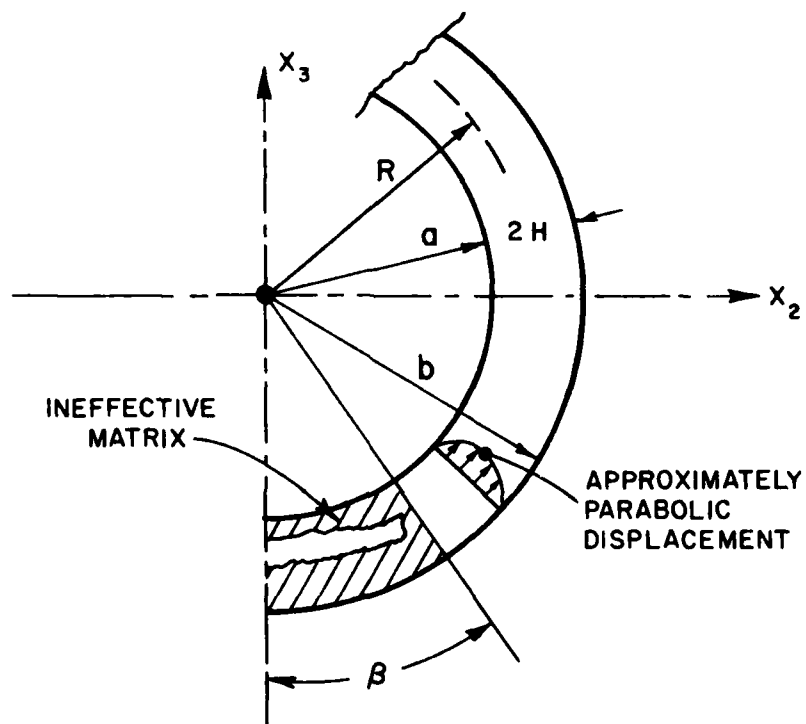


Figure 7. Portion of matrix shell with crack.

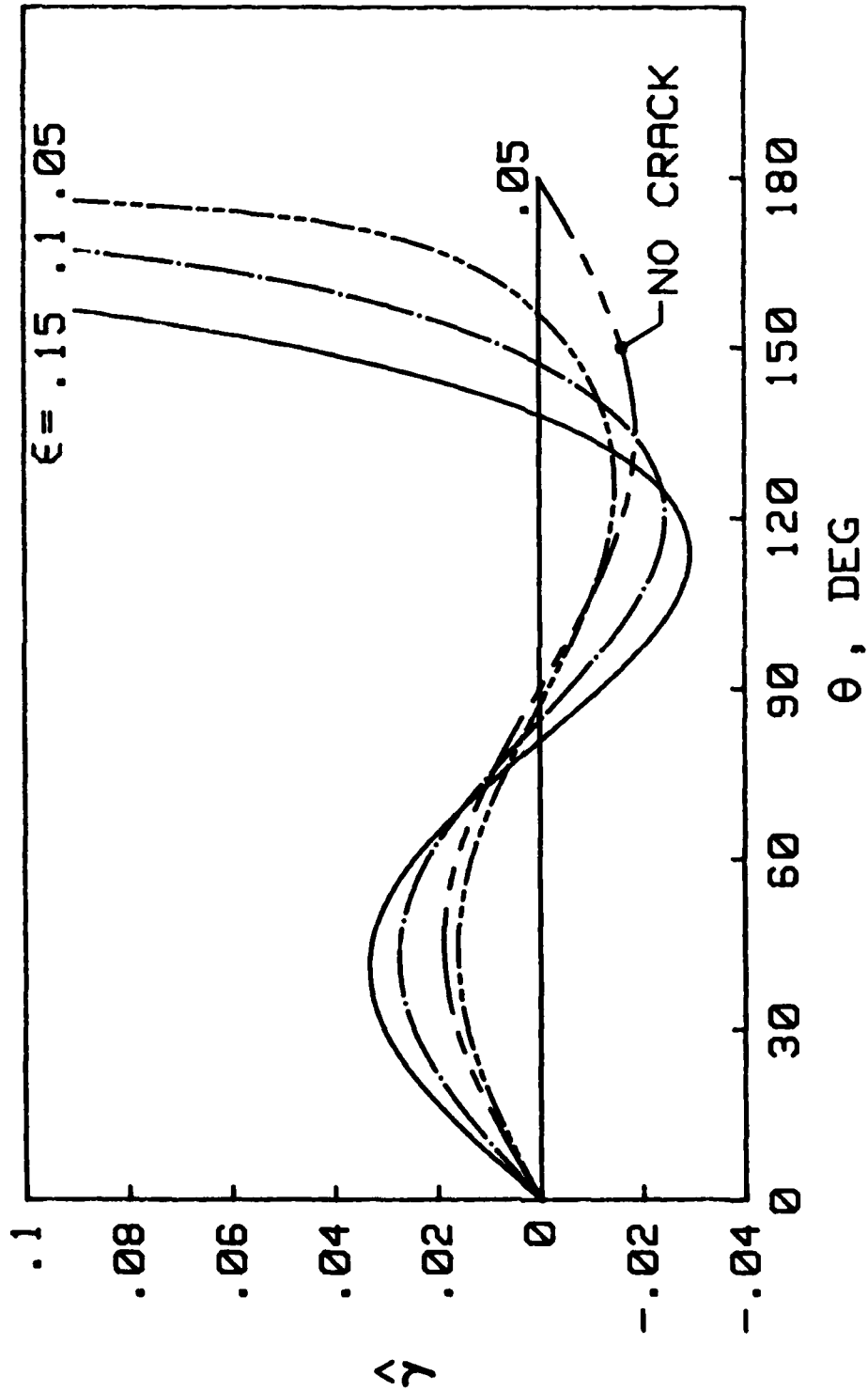


Figure 8. Variation of matrix shear strain measure with latitudinal angle.

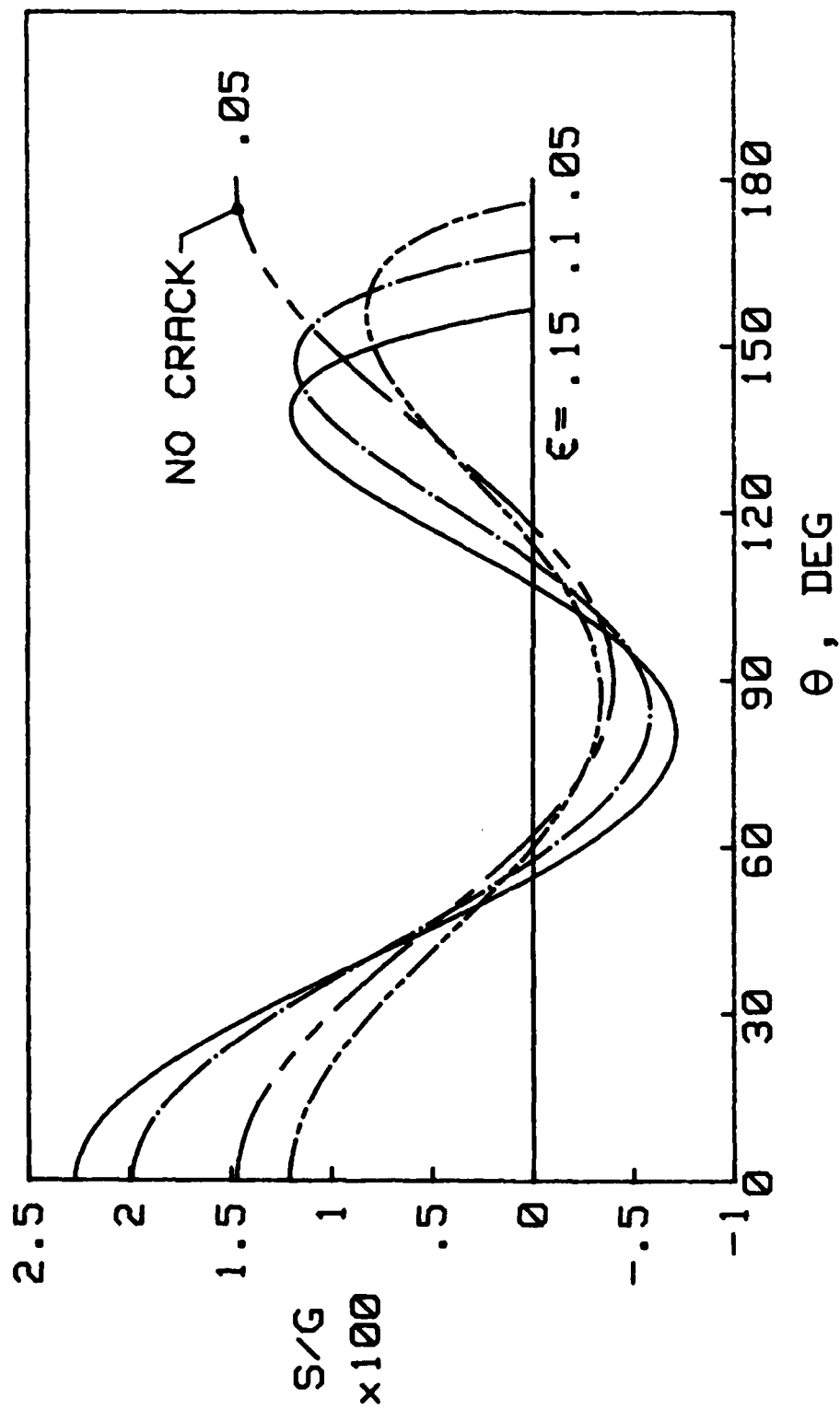


Figure 9. Variation of matrix mean stress measure with latitudinal angle.

END
FILMED

4-86

DTIC